

Ar 2p spectroscopy of free argon clusters

E. Rühl, C. Heinzl, A. P. Hitchcock,^{a)} and H. Baumgärtel
*Institut für Physikalische und Theoretische Chemie, Freie Universität Berlin, Takustr. 3, D-1000,
Berlin 33, Germany*

(Received 8 July 1992; accepted 26 October 1992)

Total electron and total and partial ion yield spectra of Ar clusters (with average size up to 600 ± 200) in the region of Ar 2p excitation have been measured using synchrotron radiation and time-of-flight mass spectrometry. As the average cluster size increases, the x-ray absorption spectrum changes systematically from that of atomic Ar to that of solid Ar. The shape of the Ar $2p_{3/2} \rightarrow 4s$ region is found to be a sensitive monitor of the cluster sizes present in a molecular beam of Ar clusters. Extended x-ray absorption fine structure (EXAFS) is detected in the spectra of the larger clusters. There is a strong correlation between the intensity of the components of the Ar $2p_{3/2} \rightarrow 4s$ signal associated with clusters and the intensity of the Fourier filtered first shell Ar 2p EXAFS signal. A low amplitude, high frequency fine structure is observed in the Ar 2p continuum of the heaviest clusters which corresponds closely to that observed in solid Ar. This signal develops with cluster size more slowly than the Ar 2p EXAFS and 4s exciton signals.

I. INTRODUCTION

Although inner-shell excitation by inelastic electron scattering or by x-ray absorption is being used extensively for studies of stable gases, surface adsorbates, and solids, the field of core excitation and decay studies of molecular beams consisting of homogeneous or heterogeneous clusters of atoms and molecules is in its infancy. This paper reports extensions of recently published studies of core-level excitation¹ and ionic fragmentation² of argon clusters. Studies of a range of atomic and molecular clusters have been described recently.³ The development of a cooled nozzle has allowed the production of cluster beams with much larger average cluster sizes (\bar{N} up to 750 vs 10 in the earlier work^{1,2}). The availability of a wider range of average cluster sizes has allowed us to use Ar 2p (L_{23}) spectroscopy to follow the development of the electronic structure of clusters over essentially the whole range between the isolated atom^{4,5} and a cluster so large that its spectral characteristics become very similar to those of solid argon.⁶⁻⁸

It is widely recognized that cluster studies are useful for understanding the relationship of the geometric and electronic structure of isolated units (atoms or molecules) to that of the condensed state. Knowledge of intermediate structures aids understanding of nucleation phenomena, which are important in crystal growth, cloud formation, etc. Farges *et al.*⁹ have performed elegant studies of the size dependence of the structure of Ar_n clusters using a combination of electron diffraction and molecular dynamics. They have developed a model of the cluster structure as one involving icosahedral structures and then polyicosahedral units as the size increases. The electron diffraction pattern of Ar clusters evolves to that expected for a bulk

fcc structure [i.e., that of Ar(s)] by a size of about 700 Ar atoms. Goyal *et al.*¹⁰ have used infrared spectroscopy of SF₆ embedded in and adsorbed on Ar clusters to investigate the transformation of Ar clusters from polyicosahedral to fcc structure. Beck and Berry¹¹ have reported calculations of the structure and dynamics of small Ar clusters ($n < 20$) which give insight into the size at which liquidlike and solidlike behavior is expected.

Figure 1 presents the Ar 2p spectrum of the free atom^{4,5} in comparison to that of the crystalline solid⁶⁻⁸ Menzel and co-workers^{12,13} have discussed in detail the relationship of the atomic and solid state spectral features. The complex *ns* and *nd* Rydberg structure of the atom transforms into two excitonic lines which lie 0.9 eV to higher energy than the corresponding 4s and 3d Rydberg transitions in the atom. At the same time, the ionization threshold of the solid^{6,7,12} shifts to considerably lower energy than in the atom, although the location of the Ar 2p IP of solid Ar is not precisely known. The Ar 2p continuum of the solid differs markedly from that of the atom with the superposition of a high amplitude, low frequency oscillation which is the first shell EXAFS signal and a higher frequency lower amplitude structure whose origin has not been discussed in the literature but which is likely XANES-type structure, sensitive to both radial and angular correlations over many atomic shells. In this work photoionization and mass spectral techniques are used to measure the Ar 2p spectrum of Ar_n clusters in a supersonic molecular beam. The question we address is how the Ar 2p spectrum of argon clusters changes from that of the atom to that of the solid as the cluster size increases. Of particular interest is the evolution with cluster size of the $2p_{3/2} \rightarrow 4s$ and Ar 2p EXAFS and XANES spectral features.

Other recent studies of photoionization and photofragmentation of Ar clusters include valence ionization threshold studies using TPEPICO on Ar_n , $2 < n < 15$;¹⁴ investiga-

^{a)}Permanent address: Department of Chemistry, McMaster University, Hamilton, L8S 4M1 Canada.

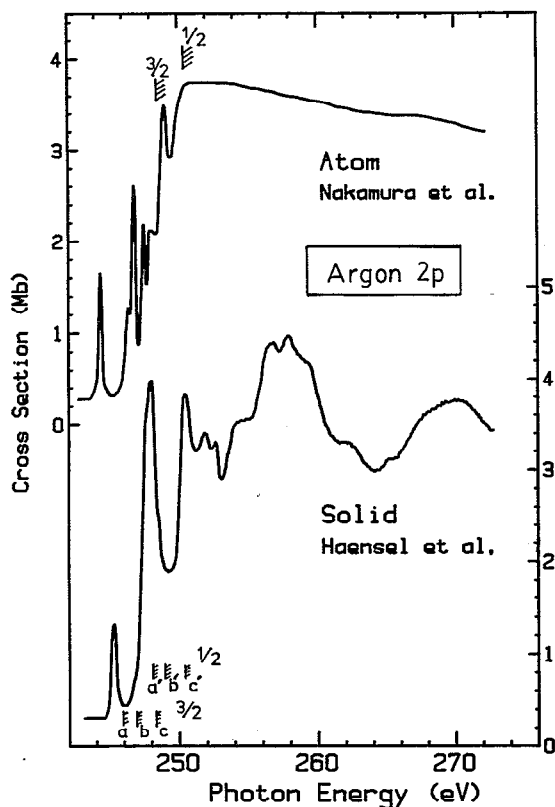


FIG. 1. Comparison of the Ar 2p spectra of atomic (Ref. 4) and solid Ar (Ref. 6). The hatched lines indicate the ionization thresholds as determined by Rydberg extrapolation (Refs. 4 and 5). Three estimates of the solid state $2p_{3/2}$ IP differing by 2.5 eV have been reported: a—Ref. 7, b—Ref. 12, and c—Ref. 37. a', b', and c' refer to the Ar $2p_{1/2}$ IPs.

tions of a metastable state around 27–29 eV believed to be specific to certain ranges of cluster size;¹⁵ investigations of the valence spectroscopy of Ar_n^+ ionic clusters.^{16–18} Wörmer *et al.*^{19,20} have recently explored the formation and confinement of Wannier excitons in studies of the UV fluorescence excitation of free Ar clusters. They find the Ar cluster must be at least four times as large as the excitonic radius in order for Wannier excitons to appear. In the area of core photoionization, total and partial ion yield Ar 2p spectra of condensed phase Ar have been reported recently for both bulk and surface monolayer Ar.^{12,13} The Ar $2p_{3/2} \rightarrow 4s$ transition in a monolayer of Ar physisorbed on Ru(001) occurs 0.5 eV below that in bulk Ar.¹² It might be expected that the shift of the corresponding transition in small Ar clusters will be similar since, in small clusters, a large fraction of the Ar atoms are at the surface. There have been studies of the core excitation spectra of Ar (and other rare gases) in high pressure bubbles injected by ion implantation and trapped in a solid.²¹ Faraci *et al.*²² have reported Ar 1s EXAFS studies of pressurized Ar clusters in Al and Si. The Ar 2p spectra of co-condensed Ar–N₂ mixtures, in which the Ar may form clusterlike structures, have also been reported.⁷ These studies provide additional insight into the structure and spectroscopy of Ar_n clusters and complement our investigation of the dependence of the

Ar 2p spectrum on the local environment of the core excited atom. Very recently Lengen *et al.*²³ have used valence shell fluorescence excitation spectroscopy to distinguish various surface and bulk sites of Xe in XeAr_n clusters.

II. EXPERIMENT

Details of the compact cluster apparatus have been presented elsewhere.^{2,3} A 5 bar stagnation pressure (p_0) behind a 50 μm variable-temperature conical nozzle was used in cluster generation. The jet then passes through a 500 μm skimmer. Down-stream pressures were ca. 4×10^{-3} Torr in the expansion region, 5×10^{-6} – 1×10^{-5} Torr in the photoionization region, and $< 1 \times 10^{-8}$ Torr just prior to the x-ray beam line. The nozzle was cooled by gravity-fed liquid nitrogen. Careful adjustment of the flow rate allowed a stability of $\pm 5^\circ$ in the nozzle temperature (T_0), as measured by a thermocouple.

The experiments were carried out using the HE-TGM2 beam line at BESSY. A few measurements were also made using the HE-TGM1 beam line. The photon energy scale was established by assuming the total electron yield (TEY) spectrum under expansion conditions of $p_0 = 1$ bar, $T_0 = 30^\circ\text{C}$ is that of the atom and calibrating the $(2p^{-1}, 4s) ^1P_{3/2}$ peak in this spectrum to 244.390 eV.⁵ The energy scale was relatively constant (± 0.1 eV) over a single fill (2–3 h) and in many cases there was no detectable shifts between fills on the same day. The stability of the energy scale with time is critical in this experiment since we are interested in measuring shifts of less than 0.1 eV in resonance position with cluster size. The spectra were normalized to the incident photon flux which was determined from the total electron yield spectrum of Kr corrected for the Kr absorption cross section. For the HE-TGM2 beam line the incident flux is very flat ($< 20\%$ variation between 240 and 320 eV) with negligible ($< 2\%$) dip at the position of the carbon K edge. The flux-normalized spectra were converted to absolute cross sections by setting the intensity of the Ar 2p continuum at 260 eV (i.e., after subtracting the underlying valence continuum) to the value of 3.2 Mb reported in Fig. 5 of Ref. 6. At this energy one is close to a node in the extended fine structure and the atom and solid have very similar cross sections.

III. RESULTS AND DISCUSSION

A. Mass spectral characterization of cluster beams

The average cluster size in the beam produced with various expansion conditions has been estimated from the stagnation pressure, nozzle temperature, and orifice dimension. These are used to calculate a reduced scaling parameter, Γ^* ,²⁴ from which \bar{N} , the average cluster size can be estimated using several different correlations reported in the literature.^{20,25} The estimated \bar{N} values differ by more than a factor of 2 (see Table I), indicative of the level of uncertainty in knowledge of cluster size and size distributions. There is a need to develop alternate procedures for monitoring cluster beams. Ar 2p spectroscopy as described below may contribute in this area.

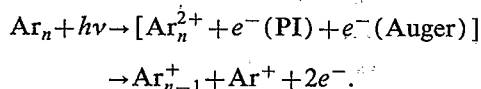
TABLE I. Predicted average cluster size (\bar{N}) for experimental expansion conditions.

T_0 (°C)	Γ^{*a}	\bar{N}^b	
		Ref. 25	Ref. 20
30	490	10	10
0	620	15	20
-10	675	18	30
-20	740	20	50
-30	810	22	80
-40	900	25	105
-50	990	35	140
-60	1100	40	175
-70	1230	50	225
-80	1380	60	270
-90	1570	70	340
-100	1790	80	430
-110	2050	120	530
-120	2380	200	750

^aReduced scaling parameter, $k \cdot d^{0.85} [\mu\text{m}] \cdot p_0 [\text{bar}] / T_0^{2.29} [\text{K}]$; where k is a constant (1.646); p_0 is the stagnation pressure, d is the orifice diameter, and T_0 is the nozzle temperature (Refs. 20 and 23).

^bPredicted for 50 μm nozzle size, $p_0=5$ bar and the indicated nozzle temperature (T_0) using the correlation outlined in the indicated references.

Figure 2 presents a selection of time-of-flight (TOF) mass spectra over the range of cluster conditions employed. They were recorded using 415 eV photon energy [above the Ar 2p ionization potential (IP)] and a 300 V, 2 μs extraction pulse with the time-of-flight potentials chosen to match the Wiley-McLaren focusing conditions.²⁶ With an expansion of $T_0=20^\circ\text{C}$, $p_0=5$ bar Γ^* is 500, corresponding to \bar{N} of 10. Even so Ar_8^+ is the largest cluster ion observed and the majority of the mass spectral features are associated with the large proportion of unclustered atoms present in the beam. At 415 eV the mass spectrum of atomic Ar is dominated by Ar^{2+} , with appreciable Ar^{3+} , some Ar^{4+} and very little Ar^+ .²⁷⁻²⁹ The multiple ionization is associated with the Auger decay of the initial Ar $2p^{-1}$ ionized state. Aside from a small signal in the 2 eV above the IP which is a post-collision interaction effect,^{1,16} Ar^+ signal above the Ar $2p_{1/2}$ IP can only arise in the atom from fluorescence decay, which is of very low probability. Thus almost all of the Ar^+ signal (and all of the Ar_n^+ signal) comes from dissociative double ionization of Ar clusters in processes of the type,³



Although symmetric charge separation occurs and recent triple coincidence (PEPIPICO) experiments have shown that it dominates the fragmentation of small clusters,³⁰ asymmetric charge separation is the dominant channel for the fragmentation of large clusters.² Since time-of-flight spectrometers discriminate against heavier mass ions (in part because of lower detector sensitivity and in part because the TAC is stopped by the earlier arrival of the lighter ion), the lighter partners in asymmetric charge separation events are detected preferentially. Thus the cation

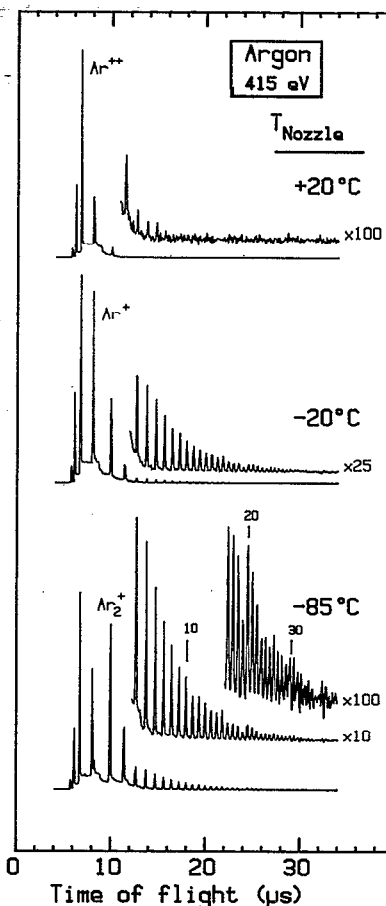


FIG. 2. Time-of-flight mass spectra of Ar cluster beams produced by 415 eV photons. The spectra were obtained using a 2 μs , 300 V extraction pulse as the start of the time scale. The stagnation pressure (p_0) was 5 bar for all three spectra with nozzle temperatures (T_0) of 20, -20, and -85 $^\circ\text{C}$.

distribution in the mass spectrum underestimates the size distribution of the neutral clusters.

Cooling the nozzle produces additional clustering, as indicated by the mass spectra of beams produced with $T_0 = -20^\circ\text{C}$ and $T_0 = -85^\circ\text{C}$ presented in Fig. 2. This immediately results in the appearance of intense Ar_n^+ signals and a large increase in the Ar^+ signal which is associated with dissociative double ionization of larger clusters. The proportion of free atoms in the beam can be estimated from the intensity of the Ar^{2+} or Ar^{3+} signals since these ions are produced primarily from Ar atoms. The largest average cluster sizes were obtained at $T_0 = -120^\circ\text{C}$, $p_0 = 5$ bar. Under these conditions the ($\text{Ar}^{2+} + \text{Ar}^{3+}$) intensity was less than 0.1% of the spectrum indicating that an almost pure cluster beam has been produced. When T_0 was below -120°C the nozzle invariably became clogged with Ar ice. Alignment of the molecular beam and the x-ray beam is critical to achieve very high cluster sensitivity since the proportion of atoms greatly increases outside the centre of the beam.

There are significant mass and kinetic energy discrimination effects in both the extraction of the photoions into the TOF MS and in the detection of ions by the channel-

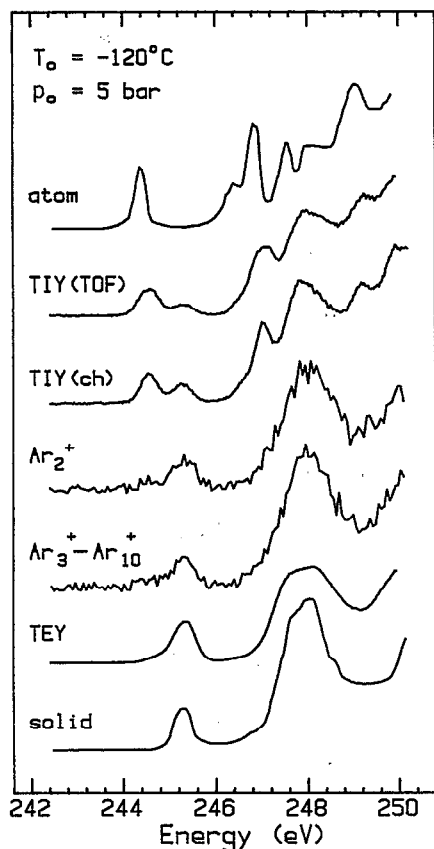


FIG. 3. Comparison of Ar 2*p* near edge spectra of the ($T_0 = -120^\circ\text{C}$, $p_0 = 5$ bar) cluster beam recorded with various total and partial yield techniques. The relative contribution of the atomic or the heavy cluster portion of the distribution of species present in the beam varies because of differing sensitivity of the detection techniques. The Ar 2*p* spectra of atomic (Ref. 4) and solid (Ref. 6) Ar are also plotted to facilitate comparison.

plate. Heavy ions and species with high kinetic energy are discriminated against. Thus the cluster ions seen in the mass spectra represent only the lower size portion of the parent neutral species in the beam. The high mass component of these spectra can be enhanced by using a longer time extraction pulse although there is a penalty in terms of degraded mass resolution and distortion of peak shapes which is seen as a background under the Ar^{++} and Ar^+ peaks in Fig. 2.

B. Total and partial ion yield spectra

In order to understand what portion of the cluster distribution contributes to a given yield spectrum we have investigated the sensitivity of the various detection techniques employed. (see Fig. 3). These include total electron yield (TEY); partial ion yield (PIY) for any mass; total ion yield (TIY) detection both with a channeltron directly adjacent to the ionization region [denoted TIY (ch)] and with the channelplate detector at the end of the time-of-flight mass spectrometer [denoted TIY (TOF)]. Figure 3 demonstrates both the limitations (in terms of statistical precision) and the benefits (in terms of selectivity) of the

different detection channels. It compares TEY, TIY (ch), TIY (TOF), and two mass selected partial ion yield (PIY) spectra—those for argon cluster cations containing between 3 and 10 argon atoms, and that of the dimer cation. All of these spectra were obtained under identical expansion conditions ($T_0 = -120^\circ\text{C}$, $p_0 = 5$ bar), corresponding to the highest degree of clustering. If there was no selectivity among the detection channels all spectra would appear the same. In fact there are large changes in the Ar 2*p* \rightarrow 4*s* transition with some modes having a greater contribution from a solidlike spectrum (4*s* exciton at 245.4 eV) and others having a greater contribution from an atomiclike spectrum (4*s* at 244.4 eV). The spectra in Fig. 3 are plotted in order of decreasing “solidlike” character and the spectra of atomic⁶ and solid⁷ argon are included at the top and bottom of the plot for comparison. Both the Ar_2^+ and the ($\text{Ar}_3^+ - \text{Ar}_{10}^+$) cluster PIY spectra are close to the spectrum of solid Ar as expected since these cluster cations arise from dissociation of larger doubly charged clusters.² It is clear that mass selected ion detection can be very beneficial at investigating the absorption spectra of specific components of a multicomponent beam. On the other hand, both total ion signals are more atomiclike, indicating that the proportion of the atomic signal is artificially enhanced because of discrimination against heavy cluster ions. If the beam really contained as high a proportion of atoms as either of the TIY spectra appear to indicate, then the TEY spectrum would have a much larger atomic contribution, since this detection channel has the least discrimination and thus best represents the spectrum integrated over the distribution of species in the beam. In addition to detection mode dependence, certain modes, particularly those based on ion detection, were also dependent on the extraction voltages employed. In all cases the conditions were chosen to optimize the sensitivity to high mass components of the beam.

C. Total electron yield spectra

Figure 4 presents total electron yield (TEY) spectra of selected cluster beams. The $T_0 = 30^\circ\text{C}$, $p_0 = 1$ bar spectrum is in good agreement with the atomic spectrum when differences in resolution are taken into account (0.4 eV in this work and 0.2 eV in the work of Nakamura *et al.*⁶). This is as expected since the beam should be mainly composed of atoms under these conditions ($\Gamma^* = 100$, $\bar{N} = 1$). As the clusters are produced with increased stagnation pressure and cooling of the nozzle, there are dramatic changes in both the discrete and continuum parts of the spectrum.

There is a systematic change in the Ar 2*p*_{3/2} \rightarrow 4*s* transition around 245 eV from the atomic 4*s* Rydberg line to the solid 4*s* exciton peak over this range of cluster sizes. Similarly there is a conversion from a complex overlap of atomic ($2p_{1/2}^{-1}4s$), ($\text{Ar}_{3/2}^{-1}3d$) Rydberg transitions around 248 eV, to a 3*d* exciton feature in Ar(s) as the average cluster size increases. This transformation occurs in parallel to the changes in the 4*s* region. The clarity with which these changes are detected is remarkable since the TEY signal is an average over all species in the cluster beam. This is further evidence that the beam is mostly composed

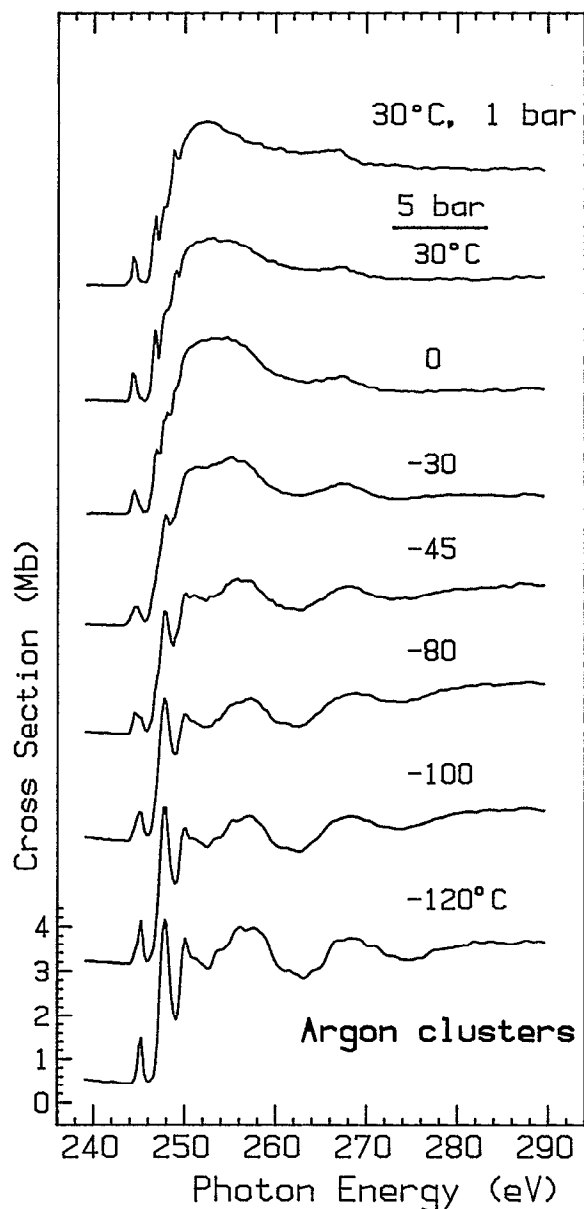


FIG. 4. Total electron yield (TEY) spectra of Ar_n clusters under the indicated beam conditions. The spectra have been converted to absolute photoabsorption cross sections based on literature values for atomic $2p$ ionization (Ref. 6). They are plotted on a common intensity scale.

of large clusters at the coldest nozzle temperature and that there was good alignment of the synchrotron radiation and the Ar cluster beams. The extended x-ray absorption fine structure features (EXAFS), which are the broad oscillations peaking at 258, 270, and 283 eV, are detectible down to average cluster sizes of about 50 ± 30 . The broad peak at 268 eV seen in the upper two curves of Fig. 4 is also seen in the spectrum of atomic Ar (see Fig. 1) and is likely a (LM) double excitation structure. The amplitude of the EXAFS signal increases with increasing average cluster size. The EXAFS amplitude saturates as the transformation from the atomic Rydberg line to the $4s$ exciton of the solid is completed. The spectra in Fig. 4 represent only half of the temperatures sampled and about one quarter of the

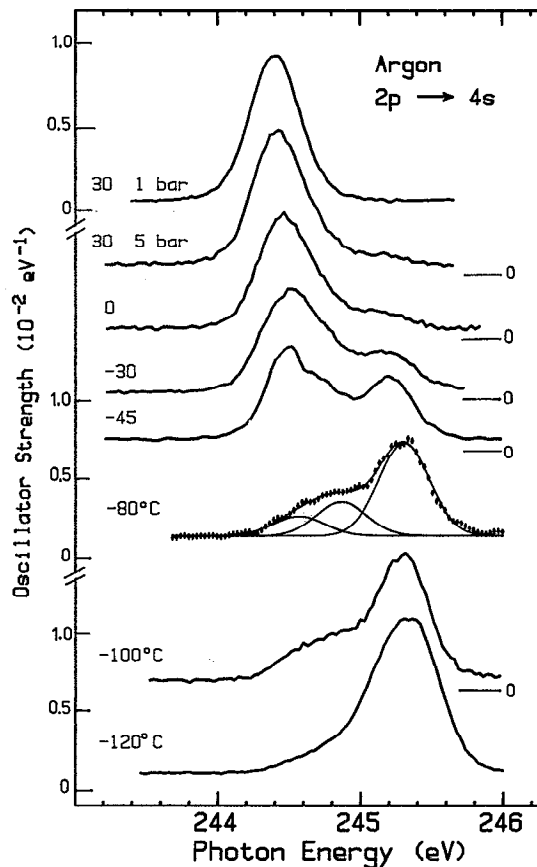


FIG. 5. Expanded presentation on an oscillator strength scale of the Ar $2p_{3/2} \rightarrow 4s$ transition. All spectra are plotted on a common scale. The zero for each curve is indicated. A curve fit to three Gaussian peaks is shown for the spectrum obtained with $T_0 = -80^\circ\text{C}$. Each spectrum was analyzed with a similar three component fit to provide the data tabulated in Table II.

total number of TEY spectra recorded in this study. Thus the presentation is illustrative rather than exhaustive. The other TEY data fully confirm the results reported in Figs. 4.

D. Detailed analysis of the $4s$ and $3d$ region of the TEY spectra

Figure 5 is an expanded presentation of the $4s$ region of these TEY spectra, plotted on an absolute intensity scale in oscillator strength units ($1 \text{ Mb} = 109.75 \text{ eV}^{-1}$) determined by the continuum normalization. The variance of the integrated $4s$ oscillator strength (peak area) is 16% for all of these spectra. The preservation and perhaps small increase of the $4s$ intensity with increasing cluster size (see top panel of Fig. 6) is evidence that the atomic Rydberg signal does not disappear but rather is converted into an alternate signal which eventually becomes the $4s$ exciton of solid Ar. This is a very clear resolution of a long standing discussion about the fate of Rydberg states in condensed phases—that is, whether the Rydberg states of isolated atoms and molecules disappear or are transformed to other entities in the condensed state.³¹

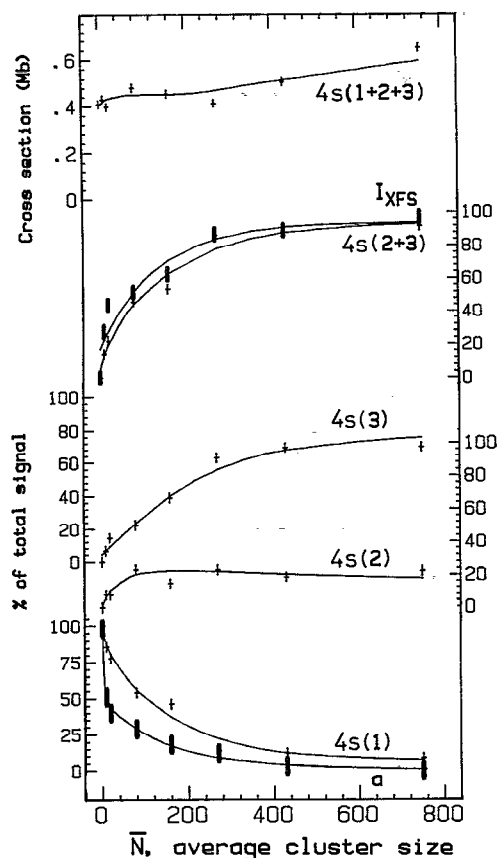


FIG. 6. (Top panel) Variation with average cluster size of the total Ar $2p_{3/2} \rightarrow 4s$ cross section. The \bar{N} values are estimated using the relationship reported by Farges *et al.* (Ref. 9). The second panel compares $[4s(2+3)]$, the sum of the relative intensity of the second and third components of the $4s$ region expressed as a percent of the total $4s$ signal, and I_{XFS} , the amplitude of the Fourier filtered first shell Ar $2p$ EXAFS. The EXAFS amplitude was scaled to that of $4s(2+3)$. The lower three panels indicate the cluster size dependence of the three $4s$ component signals, expressed as a percent of the total signal. The curve labeled a in the lowest panel is the intensity of the $(Ar^{2+} + Ar^{3+})$ signal expressed as a percent of the total (noncoincident) mass spectral signal. This signal is representative of the atomic content of the molecular beam. The difference between the $(Ar^{2+} + Ar^{3+})$ and $4s(1)$ signal indicates that the $4s(1)$ signal at lower nozzle temperatures contains cluster contributions, consistent with the observed shifts in the $4s(1)$ energy. In all cases the solid lines are the result of exponential or polynomial fits to the data points. These do not have any theoretical significance but are included as guides to the eye.

The spectra of Fig. 5 (and others) have been analyzed with Gaussian curve fits. A minimum of 3 components are needed to explain the peak shapes of spectra recorded for nozzle temperatures between -30 and -100 °C. Since the TEY signal contains contributions from all cluster sizes present for a given expansion, one might expect a many-component spectrum with poorly defined structure. However three components can provide a satisfactory fit to all of the $4s$ spectra. One sample curve fit is presented in Fig. 5 while the component energies, peak widths, and cross sections derived from the fits are summarized in Table II. This analysis allows a quantitative evaluation of the redistribution from an “atomiclike” signal [called $4s(1)$],

through an “intermediate-clusterlike” signal [$4s(2)$] to a “solidlike” signal [$4s(3)$].

The energies of each of the three Ar $2p \rightarrow 4s$ components increase by ~ 0.35 eV over the sequence of decreasing nozzle temperature and thus increasing cluster sizes. Since small shifts in the monochromator energy scale may occur or nozzle misalignment may change the composition of the photoionized beam and thus the spectral shapes, we have verified the results in three different series of measurements. This has shown that the shifts in $4s$ peak energies are time independent. However it can not be completely excluded that the shifts have some instrumental component since they are only slightly larger than the uncertainties in the experimental energy scale. More accurate calibrations in combination with higher photon energy resolution are highly desirable.

A systematic increase in the energy of the 2nd and 3rd components with \bar{N} is readily understandable but the increase in the lowest energy component was puzzling at first, since we had initially assumed this was the Ar $2p_{3/2} \rightarrow 4s$ transition in the atoms present in the molecular beam. However under more strongly clustered conditions there is very little evidence for atoms in the mass spectrum and yet a low lying $4s$ signal remains around 244.5 eV. The upward shift in the energy of the $4s(1)$ signal can be understood if one assumes this component includes the $4s$ signal from small clusters and/or from Ar atoms at the surfaces of larger clusters, in addition to the $4s$ signal of the atom. With this outlook, the shift in the energy of the first component is then interpretable in terms of changing proportions of atoms and small clusters. In our previous work¹ the $4s$ peak in the Ar_2^+ partial ion yield spectrum for \bar{N} of 10 ($\Gamma^* = 500$) was observed to occur 0.35(9) eV above that of the atom, i.e., at 244.7(1) eV. According to Fig. 2 the mass selected ion spectrum of Ar_2^+ is associated with the cluster species present because of the predominance of asymmetric charge transfer.² Thus a 0.35 eV shift relative to atomic Ar is expected for small clusters. Since most of the atoms are at the surface in small clusters, it is also possible that atoms at the surface of larger clusters have their $2p \rightarrow 4s$ transition around 244.7 eV. A distinct valence shell spectral feature associated with Xe in surface sites in $XeAr_n$ clusters has recently been identified,²³ supporting our view that surface shifts in rare gas clusters can be significant. For expansion conditions in which there is still an appreciable atomic content the $4s(1)$ signal occurs close to the value for the atom and the small cluster signal gives rise to a distinct second component. The $4s(2)$ component is clearly seen through most of the series of spectra.

For smaller cluster sizes the $4s(2)$ energy matches the energy of the Ar $2p \rightarrow 4s$ transition in the Ar_2^+ yield measured previously under $\bar{N} = 10$ conditions.¹ As the cluster size increases, the position of the second line shifts closer to 245.0 eV similar to the position of the $4s(3)$ component under weakly clustering conditions. The $4s(2)$ energy is very similar to that of the Ar $2p_{3/2} \rightarrow 4s$ transition in a monolayer of Ar physisorbed on Ru(001).¹² This is consistent with attributing the $4s(2)$ component not only to small clusters, but also to Ar in a reduced bonding envi-

TABLE II. Energies (eV), cross sections (Mb), and widths (eV) of the three Gaussian components fit to the Ar $2p_{3/2} \rightarrow 4s$ structure.

Sample		Component #								
		1			2			3		
T_0 (P_0)	\bar{N}	E (eV)	I (Mb)	Width	E (eV)	I (Mb)	Width	E (eV)	I (Mb)	Width
Atomic ^a		244.39(1)		0.38	0.27					
30 (1 bar) ^b	1	244.38 ^c	0.41	0.43						
30	10	244.42	0.37	0.42	244.77	0.033	0.30	245.13	0.028	0.40
0	15–20	244.46	0.31	0.41	244.77	0.030	0.27	245.10	0.058	0.48
–30	22–80	244.47	0.26	(0.42) ^d	244.78	0.113	(0.42)	245.22	0.108	(0.42)
–45	30–160	244.51	0.21	0.36	244.83	0.067	0.26	245.21	0.177	0.42
–80	60–270	244.57	0.057	(0.42)	244.86	0.096	(0.42)	245.30	0.26	(0.42)
–100	80–430	244.55	0.061	0.35	244.87	0.095	0.37	245.30	0.35	0.42
–120	200–750	244.64	0.054	(0.48)	245.07	0.145	(0.48)	245.39	0.45	(0.48)
Solid ^e	∞							245.3(1) ^f	0.50	0.45

^aFrom the electron energy loss spectrum reported in the literature (Ref. 5). The cross section was determined from normalization of the digitized spectrum in the Ar $2p$ continuum.

^b $P_0 = 5$ bar except for this entry.

^cThe energy scale was calibrated using the $2p_{1/2} \rightarrow 4s$ transition of the atom [244.390 (Ref. 5)] several times through the sequence of measurements. Shifts of up to 0.2 eV were found between recalibrations so that some of the shifts with cluster size may be instrumental in origin. See the text for further discussion.

^dGaussian widths in brackets were fixed during the nonlinear least-squares fit.

^eFrom total electron yield measurement on bulk Ar(*s*) reported in the literature (Ref. 6).

^fAverage of reported values: 245.2 (Ref. 7) and 245.4 (Ref. 12). The cross section was determined from normalization of the digitized spectrum in the Ar $2p$ continuum.

ronment such as that at the surface of larger clusters. Component 3 has energies which increase from 245.1 to 245.4 eV with increasing \bar{N} . The highest value is very close to that reported for the $4s$ exciton in solid argon.^{7,12,13}

The Ar $2p_{3/2} \rightarrow 4s$ line in the Ar $2p$ TEY spectrum at $T_0 = -120$ °C is very similar to that of the $4s$ exciton in solid Ar,⁷ as expected from the overall similarity of its spectrum with that of the solid (see Fig. 3). Since the $4s(3)$ energy systematically increases, it appears that the $4s$ excitonic energy is dependent on the cluster size. Cluster studies provide a means for an accurate evaluation of the difference in atomic and solid state $2p \rightarrow 4s$ energies since detection modes specific for each component can be chosen and acquired from the identical beam in a single scan. When combined with threshold photoelectron measurements of the same cluster beam accurate excitonic binding energies can be evaluated. Given the wide range in the published estimates of the IP of solid Ar and thus uncertainty in the excitonic binding energy, such studies could be very important in advancing our understanding of excitons in rare gas solids.³²

Wörmer *et al.*^{19,20,25} have studied the development with size of Wannier excitons in the valence shell fluorescence excitation spectra of neutral clusters. Quite a large cluster (> 2000 atoms) is needed to see features at the same energy as that of the $n=2$ ($3p \rightarrow 3d$) exciton in solid Ar. Since the $4s$ is much more compact than the $3d$ orbital, the Ar ($2p^{-1}, 4s$) state in the solid should develop at much smaller cluster sizes than the (Ar $3p^{-1}, 3d$) Wannier exciton, as observed. Indeed the (Ar $2p^{-1}, 4s$) exciton should probably be described as a Frenkel rather than a Wannier exciton. Interestingly the (Ar $2p^{-1}, 3d$) exciton appears at about the same cluster size as the $4s$ exciton. This indicates that the size of the compact $2p$ core orbital is more impor-

tant than the size of the much larger $4s$ or $3d$ orbital in determining the cluster size needed to support specific excitonic states. Haensel *et al.*⁷ have shown that the position of the Ar ($2p^{-1}, 4s$) exciton is constant through Ar:N₂ solid solutions ranging from 10 to 100% Ar. In contrast the (Ar $2p^{-1}, 3d$) exciton shifts to lower energy by 1.0 eV as the Ar content of the film is increased from 10% to 100%. This supports a larger spatial size of the (Ar $2p^{-1}, 3d$) exciton and thus a greater environmental sensitivity. These results have recently been reproduced in studies of mixed Ar:N₂ clusters.³³

E. Quantitative aspects: Cluster size dependence of the Ar $2p_{3/2} \rightarrow 4s$ signal

The systematic evolution of the $4s$ region is a quantitative phenomenon, as demonstrated in Fig. 6 where the contribution of each of the three components is plotted against \bar{N} values derived from the expansion conditions using the relationship of Ref. 20 (see Table I). The amplitude of the first shell EXAFS signal (extracted by Fourier filtering analysis) is also plotted against the average cluster size. This is found to give excellent agreement in trend with the $4s(2) + 4s(3)$ signal, the sum of the 2nd and 3rd components in the three-component curve fit analysis of the $4s$ region (see Fig. 5), i.e., those components for which there is a more-or-less well-defined local environment of the core-excited Ar. The EXAFS amplitude is the area of the first shell signal (2–5 Å) in the Fourier transform of the normalized EXAFS signal (see Fig. 8 and Sec. III G). The $4s(2) + 4s(3)$ and EXAFS signals clearly correlate with average cluster size and with each other. This suggests that either (or both) of these signals could be used to monitor the proportion of large clusters in an argon beam.

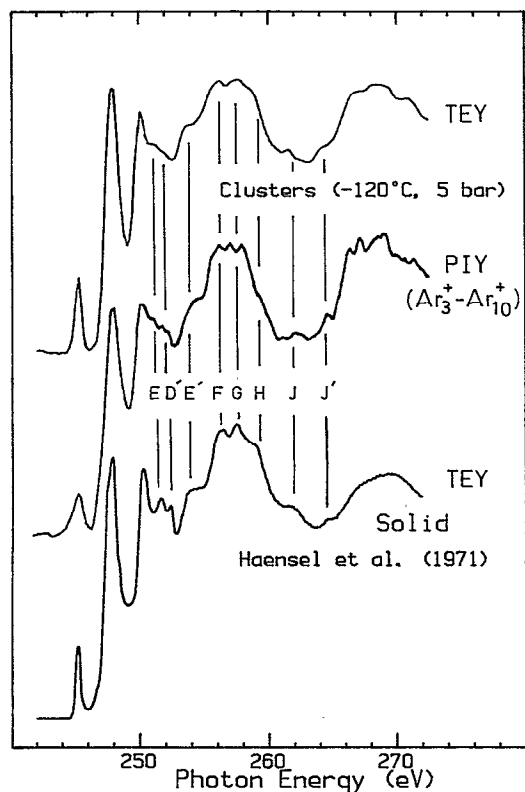


FIG. 7. Comparison of the total electron yield (TEY) and the partial ion yield (PIY) spectra of the most highly clustered beam ($T_0 = -120^\circ\text{C}$, $p_0 = 5$ bar) with that of solid Ar, digitized from Ref. 6. The PIY is the signal for Ar_3^+ , $3 < n < 10$ in the TOF mass spectrum recorded with pulse extraction. The labelling of the x-ray absorption near edge (XANES) fine structure features corresponds to that given in Ref. 6.

The sum of the Ar^{2+} and Ar^{3+} signals in the TOF mass spectrum is also plotted in Fig. 6 (curve labeled "a"). This should be proportional to the amount of atoms present in the beam since these species only arise from atomic photoionization for photon energies above 252 eV. If $4s(1)$, the first component of the $4s$ signal, only contained contributions from atomic Ar then the $\%(\text{Ar}^{2+}, \text{Ar}^{3+})$ signal should follow the cluster size dependence of that signal. Instead the $\%(\text{Ar}^{2+}, \text{Ar}^{3+})$ signal decreases with cluster size much more abruptly than the $4s(1)$ signal. This supports our interpretation that the $4s(1)$ signal arises from both atomic and surface/small cluster species, with the proportion of each changing as the cluster composition changes. This is consistent with the 0.35 eV shift to higher energy over the cluster size distribution.

Systematic spectral variations with average cluster size were obtained using all of the detection modes. However the partial and total ion signals were much more sensitive to operating parameters than the TEY and also much less representative of the true cluster distribution. Thus, although the TIY(ch) and TIY(TOF) signals also showed evolution of $4s$ and EXAFS components as a function of nozzle temperature, the spectra never approach as close to the solid spectrum as do the TEY spectra (see Fig. 3). For

this reason the $4s$ -EXAFS correlations derived from total and partial ion yield spectra are not presented, although both sets of spectra show trends qualitatively similar to those in the TEY data.

F. XANES

Figure 7 compares the Ar 2p spectrum of solid argon⁶ with that of the molecular beam under maximum clustering conditions, recorded by total electron yield (TEY) and by the partial ion yield (PIY) of Ar_3^+ to Ar_{10}^+ ions, which should be highly selective to heavier clusters.³ A very good match is found between the PIY and TEY spectra of the clusters and that of solid Ar. It is noteworthy that both of the cluster spectra exhibit a fine structure (labeled E...J' in Fig. 7, as in Ref. 6) which matches that observed in the solid state spectrum. Peak E has been attributed recently to a phenomenon dependent on the polarizability,³⁴ a property that should depend considerably on cluster size.

This fine structure may be associated with multiple scattering of the outgoing Ar 2p electron by the surrounding Ar atoms (the so-called XANES structure³⁵⁻³⁷). Such structure is sensitive to angular as well as radial correlations. It has structural sensitivity over a considerably longer range than the single scattering EXAFS fine structure. The XANES fine structure features are certainly not evident in TEY spectra of the smaller clusters produced at higher nozzle temperatures ($T_0 > -30^\circ\text{C}$), even though the EXAFS oscillations are clearly visible (see Fig. 4). In fact a distinct increase in the amplitude and a sharpening of these XANES fine structure components is seen when T_0 is decreased from -100 to -120°C . Apparently this fine structure is formed only in larger clusters, even though the single scattering first shell EXAFS signal develops under less extreme clustering conditions. Note that the vibrational amplitudes, and possibly the degree of disorder, in a given cluster likely decrease significantly as the nozzle temperature is decreased. These factors, as well as the increase in the cluster size, are probably important in the development of the XANES fine structure at the coldest nozzle conditions. The occurrence of a liquid→solid phase transformation¹¹ in the clusters may also be contributing to our observations. A detailed study of the evolution of this XANES structure as a function of average cluster size could provide additional information on cluster structure which could complement the elegant electron diffraction studies of Ar_n ($10 < n < 700$).⁹ It may be possible to analyze the XANES multiple scattering fine structure through comparison with multiple scattering theory.³⁶ This has been applied recently to obtain a complete structural determination of atomic adsorbates.³⁷ Given that the Ar 2p signal corresponds to an average over a number of cluster structures, the task of structural identification by comparison of experimental spectra with computed Ar 2p XANES for various model structures will be very laborious and perhaps partly inconclusive. Preliminary studies using the code of Pendry *et al.*³⁶ have been able to reproduce the larger amplitude XANES structures of the spectrum of solid Ar (Ref. 6) but not the finer features.

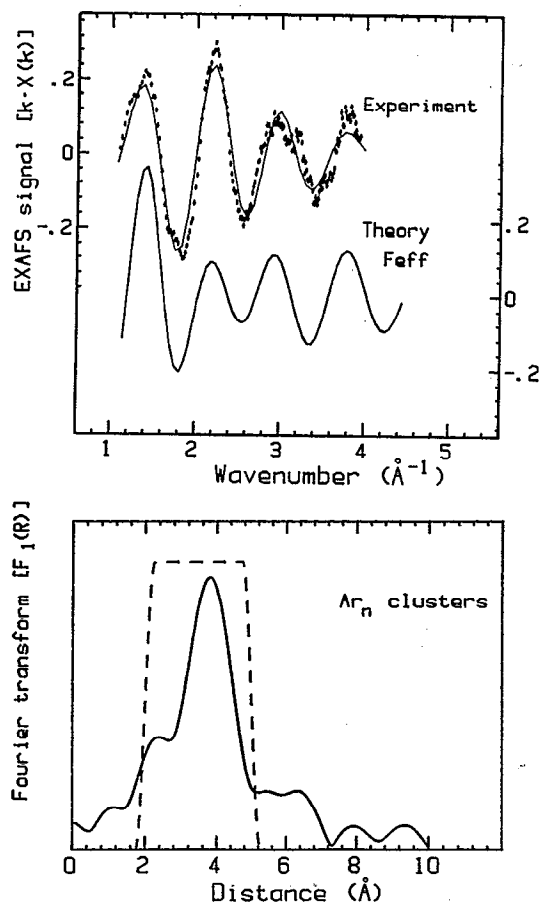


FIG. 8. Analysis of the Ar 2p EXAFS extracted from the average of nine TEY spectra, all recorded for nozzle temperatures below -60°C . The upper panel presents the background subtracted k^1 -weighted EXAFS signal (points) along with the Fourier-filtered first shell component (solid line). This is compared to that predicted for first shell EXAFS in solid Ar using the Feff spherical wave calculation (Ref. 39) with $R=3.78 \text{ \AA}$, $\sigma^2=0.04 \text{ \AA}^2$, $N=12$, $E_0=-2 \text{ eV}$. The lower panel is the magnitude of the Fourier transform of the experimental Ar 2p EXAFS. The dotted line indicates the R range included in the reverse transform to generate the Fourier-filtered signal plotted in the upper panel.

Recently the Si-K and Ge-K spectra of a series of Si and Ge-containing molecules and solids have been investigated³⁸ to explore how inner-shell spectroscopy can be used to probe the development of extended bonding in semiconductor materials. That work has addressed the question of the range about the core excited/ionized atom which contributes to the observed spectral signal in various spectral regions: pre-edge ($< \text{IP}$) resonances; x-ray absorption near-edge fine structure (XANES) (0–20 eV photoelectron energy) and extended x-ray absorption fine structure (EXAFS) ($> 20 \text{ eV}$ above the IP). A high frequency XANES fine structure somewhat similar to the high frequency XANES component in the Ar 2p spectra of solid and large clusters of Ar, is found in the semiconductor materials but not in the small molecules. This indicates the structure is sensitive to a relatively large spatial range of structure, as is the corresponding structure in solid Ar and the larger Ar clusters.

G. Ar 2p EXAFS of Ar_n clusters

As found in the Ar_2^+ partial ion yield spectrum reported earlier,¹ the Ar 2p continuum signal in the TEY spectra is clearly EXAFS, predominantly associated with the first shell distance. Figure 8 presents an analysis of EXAFS extracted from the sum of nine TEY spectra for cluster beams created with $T_0 < -60^\circ\text{C}$ for which the EXAFS data differs in amplitude but is otherwise very similar, at least at the statistical precision of these results. An Ar–Ar first shell distance of $3.78(5) \text{ \AA}$ is found, based on the theoretical Ar–Ar phase shifts calculated for Ar 2p ionization with the Feff 4.0 spherical wave code.³⁹ This is in good agreement with the nearest-neighbor distance of 3.75 \AA in solid Ar.⁶ Analysis of the TEY EXAFS from spectra at single nozzle temperatures gives distances of $3.7(1) \text{ \AA}$.

Figure 8 also compares the measured EXAFS signal with that predicted by Feff spherical wave calculations³⁹ for the first shell contribution in solid Ar, assuming a coordination number of 12 and a Debye–Waller σ^2 term of 0.04 \AA^2 , corresponding to a relative displacement of 0.2 \AA , or 5% of the bond length. This calculation was carried out for both the Ar $2p_{3/2}$ and Ar $2p_{1/2}$ components which were then shifted by 2 eV relative to each other (to account for the spin–orbit splitting) and then summed in a 2:1 ratio. In order to get a good match to experiment in wave number domain the origin in energy space of the Feff calculation needed to be 250 eV. The IP of Ar(*s*) has been estimated to be 246 (Refs. 6 and 7), 247.1 (Ref. 40) or 248.5 (Refs. 12 and 42)—in all cases several eV below the gas phase IP. Since the IP of large clusters is expected to be similar to the solid state IP, this Feff origin corresponds to an inner potential (E_0) of about -2 eV . Since E_0 can be as large as -15 eV , the -2 eV value is very reasonable. The positions and amplitudes of the Feff calculated oscillations are similar to experiment although the intensity at 2.2 \AA^{-1} is underestimated. The relatively large Debye–Waller term indicates either that there are large amplitude motions in the clusters, or (more likely) that the distribution of different sizes and structures is equivalent to a high degree of static disorder. The agreement between the experimental EXAFS data and that predicted using the McKale curved wave phases and amplitudes⁴² was significantly worse than that predicted by Feff, particularly for wave numbers below 3 \AA^{-1} .

Does our data show any evolution in the mean Ar–Ar distance with increasing cluster size? The largest difference would be expected to occur between the dimer and larger clusters. We examined the Ar 2p EXAFS in the Ar^+ PIY spectrum recorded under expansion conditions where the beam is expected to have a large proportion of dimers [$p_0 = 3 \text{ bar}$, $T_0 = 0^\circ\text{C}$ corresponding to $\Gamma^* = 370$, $\bar{N} = 4$ (Refs. 9, 20, and 25)]. The Ar^+ partial ion yield signal should be rather specific for the dimer (or more generally, the non-atomic component) since Ar 2p ionization of atomic Ar results in mainly Ar^{2+} (see Fig. 2). The Ar–Ar distance derived from the Ar 2p EXAFS in the TEY or Ar^+ PIY of the dimer could not be distinguished from that derived from the Ar 2p EXAFS of the larger clusters. We do not

consider this as a definitive result because of the limited *R*-space resolution for Ar 2*p* EXAFS associated with the short data range which is limited by the onset of Ar 2*s* excitation at 320 eV. Measurements of Ar 1*s* EXAFS (3200 eV) could be more sensitive to variations in first shell Ar–Ar distance with cluster size since this should have a longer range of usable EXAFS data and thus better *R*-space resolution. Farciá *et al.*²² have recently successfully used Ar 1*s* EXAFS to show the average first shell distance in high pressure Ar bubbles in Al is contracted 0.31(5) Å relative to unpressurized solid Ar. Thus Ar 1*s* spectroscopy of Ar_{*n*} cluster beams may provide detailed structural information. We have recently performed experiments of this type at DESY. These results show that Ar 1*s* EXAFS can be recorded over a significantly larger *k* range.⁴³ However more accurate structural results have not yet been achieved because of lower statistical precision. Ar 1*s* experiments are very challenging because the cross section for Ar 1*s* ionization is much lower than that for Ar 2*p* ionization.

IV. SUMMARY

This work clearly shows that x-ray absorption and ion yield techniques are powerful tools for studies of neutral cluster beams. Further improvement in the quantitative precision of the data is desirable and should be readily achievable. Elimination of mass discrimination effects will lead to high mass PIY spectra with much better statistical precision which should allow comparisons of the spectra of different portions of a given cluster distribution. This could help to separate the influence of size and temperature on the Ar 2*p* spectra. With improved data it may be possible to use the EXAFS and/or XANES signals to quantify the changes in the average structure of a given cluster distribution and thus characterize the evolution in geometric structure which likely occurs in parallel to the evolution in the electronic structure so clearly seen in the 4*s* region. Ideally one would like to find ways to narrow the cluster distribution in order to get structural information on one particular cluster size.

This work is one of the first cases where the evolution from atom to solid through clusters has been studied by core excitation spectroscopy. Studies of this type for Tm (Ref. 44) and Sm (Ref. 45) matrix isolated clusters have been reported recently. A theoretical treatment of the dependence of the Ar 2*p*_{3/2} → 4*s* energy on cluster size could be very helpful in providing a more detailed interpretation of these results and would be greatly welcomed. The prospect of contributing to the understanding of the size dependence of the geometric structure of Ar_{*n*} clusters⁹ awaits better quality EXAFS and perhaps detailed XANES analysis. Finally, these results clearly show that Ar 2*p* spectroscopy, particularly a line shape analysis of the 4*s* region, has great promise for cluster beam diagnostics.

ACKNOWLEDGMENTS

Financial support by BMFT Grant No. 05 5KEFXB 5 is gratefully acknowledged. A.P.H. acknowledges NATO

for a travel grant. We thank Dr. T. Tyliczszak for his generous assistance with the EXAFS analysis and for support of the analysis software (BAN—available from Tolmar Instruments, Hamilton, Ont. Canada L8V 3A9) and Dr. P. Aebi for carrying out the trial multiple scattering calculations.

- ¹E. Rühl, H. W. Jochims, C. Schmale, E. Biller, A. P. Hitchcock, and H. Baumgärtel, *Chem. Phys. Lett.* **178**, 558 (1991).
- ²E. Rühl, H. W. Jochims, C. Schmale, E. Biller, M. Simon, and H. Baumgärtel, *J. Chem. Phys.* **95**, 6544 (1991).
- ³E. Rühl, *Ber. Bunsenges Phys. Chem.* (1992) (in press); E. Rühl, C. Schmale, H. W. Jochims, E. Biller, R. Locht, A. P. Hitchcock, and H. Baumgärtel, *Particles and Fields Ser. 49. Synchrotron Radiation and Dynamic Phenomena* [AIP Conf. Proc. No. 258 (AIP, New York, 1992)], p. 230.
- ⁴M. Nakamura, M. Sasanuma, S. Sato, M. Watanabe, H. Yamashita, Y. Iguchi, A. Ejiri, A. Nakai, S. Yamaguchi, T. Sagawa, Y. Nakai, and T. Oshio, *Phys. Rev. Lett.* **21**, 1303 (1968).
- ⁵G. C. King, M. Tronc, F. H. Read, and R. C. Bradford, *J. Phys. B* **10**, 2479 (1977).
- ⁶R. Haensel, G. Keitel, N. Kosuch, U. Nielsen, and P. Schreiber, *J. Phys. (Paris) C* **4**, 236 (1971).
- ⁷R. Haensel, N. Kosuch, U. Nielsen, U. Rössler, and B. Sonntag, *Phys. Rev. B* **7**, 1577 (1973).
- ⁸W. Niemann, W. Malzfeldt, P. Rabe, R. Haensel, and M. Lübcke, *Phys. Rev.* **35**, 1099 (1987).
- ⁹J. Farges, M. F. de Feraudy, B. Raoult, and G. Torchet, *J. Chem. Phys.* **78**, 5067 (1983); **84**, 3491 (1986).
- ¹⁰S. Goyal, G. N. Robinson, D. L. Schutt, and G. Scoles, *J. Phys. Chem.* **95**, 4186 (1991).
- ¹¹T. L. Beck and R. S. Berry, *J. Chem. Phys.* **88**, 3910 (1988).
- ¹²D. Menzel, *Appl. Phys. A* **51**, 163 (1990).
- ¹³G. Röcker, P. Feulner, R. Scheuerer, L. Zhu, and D. Menzel, *Phys. Scripta* **41**, 1014 (1990).
- ¹⁴J. Krauss, J. de Vries, H. Steger, E. Kaiser, B. Kamke, and W. Kamke, *Z. Phys. D* **20**, 29 (1991).
- ¹⁵H. Steger, J. de Vries, W. Kamke, and I. V. Hertel, *Z. Phys. D* **21**, 85 (1991).
- ¹⁶W. Eberhardt, S. Bernstorff, H. W. Jochims, S. B. Whitfield, and B. Crasemann, *Phys. Rev. A* **38**, 3808 (1988).
- ¹⁷T. Nagata, J. Hirokawa, and T. Kondow, *Chem. Phys. Lett.* **176**, 526 (1991).
- ¹⁸H. U. Bohmer and S. D. Peyerhimoff, *Z. Phys. D* **11**, 239 (1989).
- ¹⁹J. Wörmer, M. Joppien, G. Zimmerer, and T. Möller, *Phys. Rev. Lett.* **67**, 2053 (1991).
- ²⁰J. Wörmer, V. Guzielski, J. Stapelfeldt, G. Zimmerer, and T. Möller, *Phys. Scripta* **41**, 490 (1990).
- ²¹Z. Tan, J. I. Budnick, D. M. Pease, and F. Namavar, *Phys. Rev. B* **43**, 1987 (1991).
- ²²G. Faracia, S. La Rosa, A. R. Pennisi, S. Mobilio, and G. Tourillon, *Phys. Rev. B* **43**, 9962 (1991).
- ²³M. Lengen, M. Joppien, R. Müller, J. Wörmer, and T. Möller, *Phys. Rev. Lett.* **68**, 2362 (1992).
- ²⁴O. F. Hagen, *Z. Phys. D* **4**, 291 (1987).
- ²⁵J. Wörmer, Ph.D. thesis, University of Hamburg, Hamburg, 1990.
- ²⁶W. C. Wiley and I. H. McLaren, *Rev. Sci. Instrum.* **26**, 1150 (1955).
- ²⁷M. J. Van der Wiel and G. Wiebes, *Physica* **53**, 225 (1971); Th.M. El-Sherbini and M. J. Van der Wiel, *ibid.* **62**, 119 (1972).
- ²⁸T. Hayaishi, Y. Morioka, Y. Kageyama, M. Watanabe, I. H. Suzuki, A. Mukuni, G. Isoyama, S. Asaoka, and M. Nakamura, *J. Phys. B* **17**, 3511 (1984).
- ²⁹P. A. Heimann, D. W. Lindle, T. A. Ferrett, S. H. Liu, L. J. Medhurst, M. N. Piancastelli, D. A. Shirley, U. Becker, H. G. Kerkhoff, B. Langer, D. Szostak, and R. Wehlitz, *J. Phys. B* **20**, 5005 (1987).
- ³⁰E. Rühl, C. Schmale, P. Morin, M. Lavollée, and H. Baumgärtel (to be published).
- ³¹M. B. Robin, *Higher Excited States of Polyatomic Molecules* (Academic, New York), Vol. 1,2 (1975), Vol. 3 (1985).
- ³²G. Zimmerer, *Creation, Motion and Decay of Excitons in Rare Gas Solids*, in *Excited State Spectroscopy in Solids* edited by U. Grassano (North-Holland, Amsterdam, 1987).

- ³³E. Rühl, C. Heinzl, and H. Baumgärtel (to be published).
- ³⁴A. A. Pavlychev and A. Barry, *Phys. Scripta* **41**, 157 (1990).
- ³⁵A. Bianconi, in *X-ray Absorption: Principles, Applications and Techniques*, edited by D. C. Koningsberger and R. Prins (Wiley, New York, 1988).
- ³⁶D. D. Vvedensky, D. K. Saldin, and J. B. Pendry, *Comp. Phys. Commun.* **40**, 421 (1986).
- ³⁷M. Pedio, L. Becker, B. Hillert, S. D'Addato, and J. Haase, *Phys. Rev. B* **41**, 7462 (1990).
- ³⁸A. P. Hitchcock, P. Aebi, T. Tyliczszak, T. K. Sham, K. M. Baines, J. Xiong, K. A. Mueller, J. M. Chen, X. H. Feng, B. X. Yang, T. E. Jackman, J.-M. Baribeau, and Z. H. Lu, *Surf. Sci.* (submitted).
- ³⁹J. Mustre, Y. Yacoby, E. A. Stern, and J. J. Rehr, *Phys. Rev. B* **42**, 10843 (1990).
- ⁴⁰O. Björneholm, Ph.D. thesis, Uppsala University, 1992.
- ⁴¹M. Altarelli, W. Andreoni, and F. Bassani, *Sol. St. Comm.* **16**, 143 (1975).
- ⁴²A. G. McKale, B. W. Veal, A. P. Paulikas, S. K. Chan, and G. S. Knapp, *J. Am. Chem. Soc.* **110**, 3763 (1988).
- ⁴³E. Rühl, C. Heinzl, A. P. Hitchcock, H. Baumgärtel, H. Schmelz, C. Reynaud, W. Drube, and R. Frahm (unpublished).
- ⁴⁴C. Blanchard, J. M. Esteva, R. C. Karnatak, J. P. Connerade, U. Kuetsgens, and J. Hormes, *J. Phys. B* **22**, L575 (1989).
- ⁴⁵C. Blanchard, E. Bouisset, J. M. Esteva, R. C. Karnatak, B. Sarpal, J. P. Connerade, U. Kuetsgens, R. Chauvistre, and J. Hormes (unpublished); C. Blanchard, *Proceedings of the Second European Conference on Synchrotron Radiation*, 1990.